JOURNAL OF BACTERIOLOGY, Aug. 2011, p. 3894–3903 Vol. 193, No. 15
0021-9193/11/$12.00 doi:10.1128/JB.00426-11

Identification of an Anchor Residue for CheA-CheY Interactions in the Chemotaxis System of *Escherichia coli*[▽]

Hemang Thakor,† Sarah Nicholas,‡ Ian M. Porter,‡ Nicole Hand, and Richard C. Stewart*

Department of Cell Biology & Molecular Genetics, University of Maryland, College Park, Maryland 20742

Received 29 March 2011/Accepted 26 May 2011

Transfer of a phosphoryl group from autophosphorylated CheA (P-CheA) to CheY is an important step in the bacterial chemotaxis signal transduction pathway. This reaction involves CheY (i) binding to the P2 domain of P-CheA and then (ii) acquiring the phosphoryl group from the P1 domain. Crystal structures indicated numerous side chain interactions at the CheY-P2 binding interface. To investigate the individual contributions of the P2 side chains involved in these contacts, we analyzed the effects of eight alanine substitution mutations on CheA-CheY binding interactions. An F214A substitution in P2 caused ~1,000-fold reduction in CheA-CheY binding affinity, while Ala substitutions at other P2 positions had small effects (E171A, E178A, and I216A) or no detectable effects (H181A, D202A, D207A, and C213A) on binding affinity. These results are discussed in relation to previous *in silico* predictions of hot-spot and anchor positions at the CheA-CheY interface. We also investigated the consequences of these mutations for chemotaxis signal transduction in living cells. CheA(F214A) was defective in mediating localization of CheY-YFP to the large clusters of signaling proteins that form at the poles of *Escherichia coli* cells, while the other CheA variants did not differ from wild-type (wt) CheA ($CheA_{wt}$) in this regard. In our set of mutants, only CheA(F214A) exhibited a markedly diminished ability to support chemotaxis in motility agar assays. Surprisingly, however, in FRET assays that monitored receptor-regulated production of phospho-CheY, CheA(F214A) (and each of the other Ala substitution mutants) performed just as well as $CheA_{wt}$. Overall, our findings indicate that F214 serves as an anchor residue at the CheA-CheY interface and makes an important contribution to the binding energy *in vitro* and *in vivo*; however, loss of this contribution does not have a large negative effect on the overall ability of the signaling pathway to modulate P-CheY levels in response to chemoattractants.

Chemotaxis in *Escherichia coli* and numerous other bacterial species involves regulation of the level of phosphorylated CheY (P-CheY) in response to spatial gradients of beneficial and harmful chemicals. P-CheY plays a crucial role in chemotaxis by enabling cells to control how frequently they change directions as they swim (2, 48, 58, 63). The level of P-CheY in a cell reflects the relative rates of phosphorylation (mediated by CheA) and dephosphorylation (mediated by CheZ) (15, 46). CheA functions as an autokinase, and this activity is regulated by membrane-spanning receptor proteins responsible for binding chemical ligands that serve as attractants or repellents (7, 16). Autophosphorylated CheA (P-CheA) serves as a phosphodonor for CheY, and the P-CheY generated by this interaction can bind to the switch component of the flagellar motor, inducing changes in cell swimming direction by promoting changes in the direction of flagellar rotation (41, 65, 66). This sequence of events provides a signal transduction pathway that allows the chemotaxis receptor proteins to regulate cell swimming pattern in response to the concentrations of attractants and repellents. This regulation takes place rapidly, as indicated by the ability of cells to respond to chemostimuli within 50 to 200 milliseconds (5, 22, 51).

CheA autophosphorylation results in covalent attachment of a phosphoryl group (—PO_3^{2-}), donated by ATP, to imidazole Nε of the CheA H48 side chain (72). During the CheA → CheY phosphotransfer reaction, CheY catalyzes the transfer of this phosphoryl group to its D57 side chain (42). This reaction is rapid (k_{cat}, ~800 s^{-1} at 25°C) and involves CheY interacting with two distinct domains of CheA, P1 and P2 (Fig. 1) (53, 54). P2 provides a docking site for rapid binding and dissociation of CheY (55). P2 is connected to P1 by a flexible linker, and so binding of CheY to P2 is thought to enhance the rate of phosphotransfer by tethering CheY in close proximity to the P1 phospho-histidine (73). In previous work, we demonstrated that genetic excision of the P2 domain from CheA dramatically slows the kinetics of CheA → CheY phosphotransfer *in vitro* and that this has a detrimental effect on the chemotaxis ability of cells (54). In addition, we demonstrated that binding of CheY to P2 of CheA is very rapid, reflecting, in part, favorable electrostatic interactions (55).

Here we used alanine-scanning mutagenesis to identify P2 residues that make important contributions to its binding interface with CheY and to assess whether loss of these contributions affects phosphotransfer kinetics and the overall abilities of the chemotaxis signaling pathway. We chose mutation sites based on the crystal structures of the *E. coli* CheY-P2 complex (33, 64) and targeted residues that appeared to mediate protein-protein contacts. The locations of these sites are shown in the three-dimensional structure of the P2-CheY complex (Fig. 1B). Another way of visualizing binding in-

* Corresponding author. Mailing address: Department of Cell Biology and Molecular Genetics, Microbiology Building (231), University of Maryland, College Park, MD 20742. Phone: (301) 405-5475. Fax: (301) 314-9489. E-mail: alec@umd.edu.

† Present address: Department of Biochemistry and Molecular & Cellular Biology, Georgetown University Medical Center, Washington, DC 20057.

‡ Present address: University of Maryland School of Medicine, Baltimore, MD 21201.

▽ Published ahead of print on 3 June 2011.

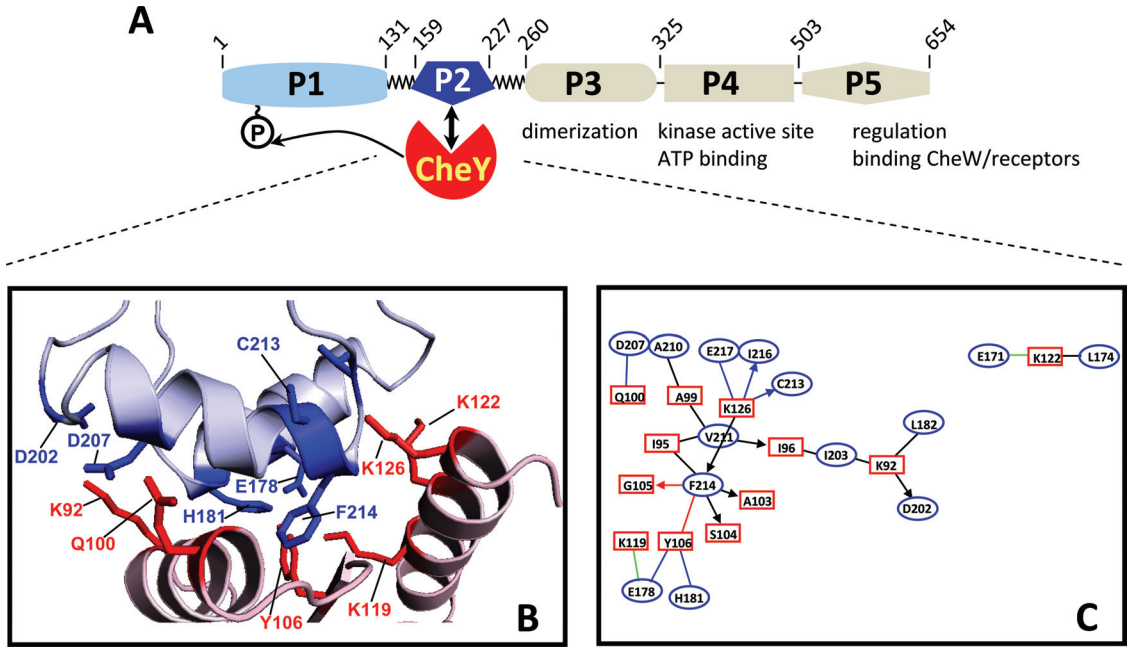

FIG. 1. Domain organization of CheA and structure of the CheA-CheY interface. (A) CheA is composed of five structural domains (P1 to P5); each plays a distinct functional role (4). The P2 domain serves as a binding site for CheY and CheB (27), and the structure of CheY-P2 complexes has been solved using X-ray crystallography (33, 64). The CheY-P2 interface from one such crystal structure is shown in panel B, highlighting the locations of side chains thought to function as protein-protein contact points. The CheY backbone cartoon is colored light pink, and important contact residues (including side chains) are colored red; the P2 backbone is colored light blue, and important contact residues are dark blue (drawn using PyMol and coordinates from PDB 1EAY). (C) Cluster analysis diagram (40) of proposed CheY-P2 contact positions generated using the AquaProt Web server at the Weizmann Institute (39) (http://bioinfo.weizmann.ac.il/aquaprot/) to analyze the P2-CheY interface (subunits A and C of PDB structure 1EAY). CheY residues are shown in red-outlined rectangles, and P2 residues are shown in blue-outlined ovals. Black lines represent proposed van der Waals contacts, blue lines represent H bonds, green lines represent favorable electrostatic interactions, and red lines indicate aromatic bonding interactions; for interactions involving backbone atoms, the arrows point toward the residues that provide the backbone atoms.

terfaces is to portray them (in two dimensions) as a cluster diagram (Fig. 1C).

MATERIALS AND METHODS

Bacterial strains and plasmids. *E. coli* strain NH1 was constructed by introducing an in-frame deletion of *cheYZ* coding sequences into Δ*cheA* strain RP9535 (30) in accordance with the procedure of Datsenko and Wanner (12). Selection for plasmids was accomplished using ampicillin (100 μg ml^{-1}), chloramphenicol (40 μg ml^{-1}), or kanamycin (50 μg ml^{-1}). Translational fusions *cheY-eyfp* and *cheZ-ecfp* were constructed as described previously (50), except that the *eyfp* and *ecfp* coding sequences each carried an A206K mutation to minimize direct interaction of yellow fluorescent protein (YFP) with cyan fluorescent protein (CFP) via dimerization (70). Each fusion included a four-glycine flexible linker connecting the Che protein and the fluorescent protein. *cheY-eyfp* and *cheZ-ecfp* were ligated into plasmid pKG116 (9) downstream of the *nahG* promoter using NdeI and BamHI restriction sites, generating pHK5. The parental plasmid provided the Shine-Dalgarno sequence for *cheY-eyfp*, and the *cheY-cheZ* intergenic sequence provided the ribosome binding site for *cheZ-ecfp*. This plasmid also included coding sequences for the positive regulator NahR, and so expression of the *cheY-eyfp* and *cheZ-ecfp* fusions was induced by adding sodium salicylate to the growth medium (1, 69). Expression of *cheA* alleles carried on pAH1-derived plasmids (17) was accomplished using IPTG (isopropyl-β-D-thiogalactopyranoside; 5 μM for chemotaxis assays and 1 mM for overexpression to generate cell extracts for protein purification). Site-directed mutations were introduced into *cheA* by oligonucleotide-directed mutagenesis using the GeneTailor kit from Invitrogen and oligonucleotides synthesized by Invitrogen. Mutant *cheA* alleles were moved into expression plasmid pAH1 using convenient restriction sites (NdeI and EcoRI for most mutations). This plasmid provided coding sequences for an N-terminal His_6 affinity tag that was used for CheA purification. For expression of the P2 domain of wild-type (wt) CheA ($CheA_{wt}$) and mutant CheA proteins, the coding sequences for residues 159 to 227 were PCR amplified and ligated into T7-expression system pET28a and the His_6-P2 domains were expressed in *E. coli* BL21 λDE3 host cells (55).

Protein expression and purification. CheY, CheA, and the P2 domain of CheA were purified from overproducing *E. coli* cells in accordance with published procedures (26, 55). His_6-CheY-enhanced yellow fluorescent protein (EYFP)-FLAG was purified by tandem affinity purification (Ni-nitrilotriacetic acid [NTA] followed by a FLAG antibody column). Protein concentrations were determined by a Bio-Rad protein assay, using bovine serum albumin (BSA) as the standard. CheY(M17C) was labeled with Badan as reported previously (56). Expression levels of CheY-EYFP directed by plasmid pHK5 were determined for cells grown in tryptone broth containing a range of salicylate concentrations. This involved recording fluorescence emission spectra from cell lysates and comparing the emission intensities to that of a solution of His_6-CheY-EYFP-FLAG (at a known concentration) as described previously (21).

Motility agar assays. Aliquots (2 μl) of freshly grown saturated overnight cultures were used to inoculate motility agar plates (0.3% Bacto agar, 1% tryptone, 0.5% NaCl, 100 μg ml^{-1} ampicillin, and 40 μg ml^{-1} chloramphenicol [for some experiments]). Plates were then incubated at 32°C, and swarm colony diameters were measured to allow calculation of the colony expansion rate (67). Each plate included a wild-type control (RP9535/pAH1cheA^{wt}), and this allowed us to express the rates supported by each mutant CheA protein, normalized to that observed with $CheA_{wt}$ under identical conditions (47).

FRET assays. The fluorescence resonance energy transfer (FRET) procedure was based on that described by Sourjik and Berg (51). Cells carrying two compatible plasmids (pAH1cheA and pHK5) were grown in tryptone broth (1% tryptone, 0.5% NaCl) containing ampicillin, chloramphenicol, salicylate (1 to 5 μM), and IPTG (5 μM) until they reached mid-log phase. These cells were then harvested by centrifugation (10 min at 5,000 rpm), washed twice, and resuspended in motility buffer (10 mM potassium phosphate, 0.1 mM EDTA, 100 μM L-methionine, and 100 mM sodium lactate, pH 7) at a final A_{600} of 0.4 and stored at 4°C until used (within 4 h). To initiate an assay, 3 ml of cell suspension was added to a standard 1-cm by 1-cm fluorescence cuvette equipped with a stir bar.

This was then placed in a standard spectrofluorometer (PTI QuantaMaster) with the following settings: excitation wavelength ($\lambda_{excitation}$), 425 nm (slits, 2 nm); emission wavelength ($\lambda_{emission}$), 526 nm (slits, 2 nm); temperature (*T*), 25°C (maintained in a Peltier temperature-regulated cuvette holder); integration time, 1 s. The emission signal was then monitored for 2,000 s before the cells were subjected to any chemotaxis stimuli. During this long interval, the emission signal climbed asymptotically, eventually reaching a plateau that was stable for >2 h. The signal increase during the initial 2,000-s interval could reflect folding/maturation of the EYFP/enhanced cyan fluorescent protein (ECFP) fluorophores (44) as well as response of the cells to the excitation light (68). Attempts to reduce the duration of this interval were unsuccessful and included vigorously aerating the cell suspensions prior to observation, adding inhibitors to block transcription and translation, and stirring the cell suspensions in the dark. Once the EYFP emission signal had reached a plateau, we monitored its response to successive additions of a chemoattractant (additions made using 2- to 10-μl additions of concentrated stock solutions using a P10 micropipetter). The cell samples were stirred continuously during these experiments; control experiments with fluorescent dyes indicated that the time required to achieve uniform mixing following an addition was less than 5 s. Attempts to detect FRET responses to repellent stimuli using this protocol gave inconsistent results: small FRET signal increases were observed often but not always. Attempts to uncover the underlying cause of this variability were unsuccessful.

Fluorescence microscopy. The images shown in Fig. 5 were recorded by a DS-QiMc charge-coupled device (CCD) camera mounted on a Nikon 80i microscope and using a 100× oil immersion objective, a C-FL YFP HC HISN filter cube ($\lambda_{excitation}$, 490 to 510 nm; dichroic mirror [Dm] 515LP; $\lambda_{emission}$, 520 to 550 nm), an ET CFP filter cube ($\lambda_{excitation}$, 426 to 446 nm; Dm, 455LP; $\lambda_{emission}$, 460 to 500 nm), and NIS Elements software. Cells were grown and washed as described above for FRET assays and then placed on a thin bed of 1% agarose and observed at room temperature.

Binding assays. Fluorescence-monitored binding titrations were used to define the binding affinities of wild-type and mutant CheA proteins for Badan-CheY(M17C) and the affinities of P2 (wild type and mutant) for CheY as described previously (55, 56). Protein samples were in TNKGDG buffer (50 mM Tris, 50 mM potassium glutamate, 25 mM NaCl, 0.5 mM dithiothreitol [DTT], 10% glycerol, adjusted to pH 7.0 using HCl). CheY samples were placed in a 10- by 10-mm or 10- by 4-mm cuvettes equipped with a magnetic stir bar and maintained at 8°C. To these samples, small volumes (1 to 10 μl) of concentrated CheA solutions were added, and emission spectra were recorded after each addition. Integrated emission signals (13) were analyzed using the least-squares fitting algorithm in DynaFit (25) (assuming a simple one-site binding model). Prior to analysis, results were corrected for the effects of dilution and for a small background fluorescence arising from the CheA/P2 samples.

Rapid-reaction experiments and analysis. Kinetics of phosphotransfer from P-CheA to CheY were monitored by following the decrease in intrinsic fluorescence of CheY resulting from its phosphorylation as detailed in previous work (38). CheY was mixed with P-CheA in a KinTek SF2004 stopped-flow spectrofluorometer (dead time, 2.5 milliseconds, using the Massey test reaction [8] at 8°C in buffer containing 10% glycerol to match our experimental conditions). $\lambda_{excitation}$ was set at 290 nm using a monochromator (4-nm band pass filter), and emission intensity was detected by a photomultiplier tube after passage through a 320-nm long-pass filter (WG320). Results for time courses from 10 consecutive shots (1,000 data points each) were averaged and then analyzed using the instrument software program. These experiments were performed under pseudo-first-order conditions ([CheY] at 8× [P-CheA] to simplify analysis) and at low temperature (8°C, maintained using a circulating water bath) to minimize the fraction of the reaction time course taking place in the instrument dead time.

Computer simulations. We used two approaches for modeling the effects of the F214A mutation on the chemotaxis signaling network of *E. coli*. Some simulations were carried out using KinTek Global Kinetic Explorer (20). This program assigned a set of differential equations to represent the following simple reaction scheme:

$$\text{CheA} \xrightarrow{k_A} \text{P-CheA} \underset{\text{CheY}}{\overset{k_{phos}}{\curvearrowright}} \text{CheA}, \quad \text{P-CheY} \xrightarrow{k_Z} \text{CheY}$$

We input rate constants tabulated by Vladimirov et al. (61, 62) [modified k_{phos} for CheA(F214A) simulations], and we input the Che protein concentrations determined by Li and Hazelbauer (28). These represent average intracellular concentrations of the Che proteins in *E. coli* strain RP437. For example, the estimated average intracellular concentration of CheY is 10 μM. However, it is worth noting that there is significant cell-to-cell variability within a population of genetically identical cells, such that it may be more realistic to consider a "typical cell" to harbor anywhere from 3 to 17 μM CheY (23). With the use of the k_{phos} value estimated above for $CheA_{wt}$, these CheY levels would enable CheA → CheY phosphotransfer to proceed with an observed rate constant of 200 to 500 s^{-1}. For cells utilizing CheA(F214A), the kinetics of this step would be slower: 30 to 70 s^{-1}. These KinTek Global Kinetic Explorer simulations calculated the steady-state levels of P-CheY and the kinetics for adjusting these levels in response to attractant stimuli.

Additional simulations used RapidCell (62), obtained from Nikita Vladimirov's website (http://www.rapidcell.vladimirov.de/). We used the default settings to calculate the P-CheY levels in wild-type cells exposed to a stepwise addition of 30 μM methyl-aspartate (attractant stimulus) and then removal of this attractant. Then, we modified the program to reflect the reduced phosphotransfer kinetics of CheA(F214A) and repeated the time course simulation to generate the output of Fig. 8.

RESULTS

Effects of Ala substitutions on CheA-CheY binding affinity. We engineered alanine substitutions at each of the P2 residues that had been identified in previous work as CheY contact points in the P2-CheY crystal structures generated by McEvoy et al. (33) and Welch et al. (64). We then purified each mutant version of CheA and measured the affinity of its binding interaction with Badan-labeled CheY [$CheY_{bd}$ is CheY(M17C) to which the fluorescent reporter molecule Badan had been covalently attached (56)]. This modification of CheY allowed us to monitor binding by following the enhanced emission signal of the environmentally sensitive Badan fluorophore (dimethylaminonapthlalene). For titrations of $CheY_{bd}$ with $CheA_{wt}$, an increase of ~40% in the integrated emission signal was observed at saturating CheA concentrations. The eight Ala substitution versions of CheA exhibited similar abilities to enhance the fluorescence emission signal of $CheY_{bd}$, and analysis of binding titrations (Fig. 2 and results not shown) allowed us to define the dissociation constant (K_d) for each version of CheA (Table 1). This analysis indicated that the F214A substitution caused a large decrease in binding affinity (>400-fold increase in K_d), three mutations (E171A, E178A, and I216A) had small effects (2- to 3-fold increases in K_d), and the remaining four mutations (H181A, D202A, D207A, and C213A) had no significant effect on the affinity of CheA for CheY.

The low affinity of the CheA(F214A)-CheY binding interaction made it impossible to approach saturation in titration experiments, and this limited the accuracy of the estimated binding affinity. In the experiment summarized in Fig. 2A (inset), for example, the highest CheA concentration that we could generate without excessive dilution of the Badan-CheY was only ~25% of the K_d. To extend the binding curve to higher CheA concentrations, we utilized the isolated P2 domain of CheA, which can be concentrated more extensively than full-length CheA. We analyzed binding of P2(F214A) and $P2_{wt}$ (Fig. 2B) by following the decrease in CheY intrinsic fluorescence, as described previously (45, 57). This analysis indicated a K_d of 120 ± 20 μM for P2(F214A), compared to a K_d of 0.09 ± 0.01 μM for $P2_{wt}$. These experiments with the isolated P2 domain confirmed our conclusion that F214 makes an important contribution to the binding energy of the CheA-CheY complex and indicated a value for ΔΔG (the binding energy observed with the mutant protein minus the binding energy observed with the wild-type protein) (14) of ~4 kcal/mole for the F214A substitution. Figure 3 depicts the observed

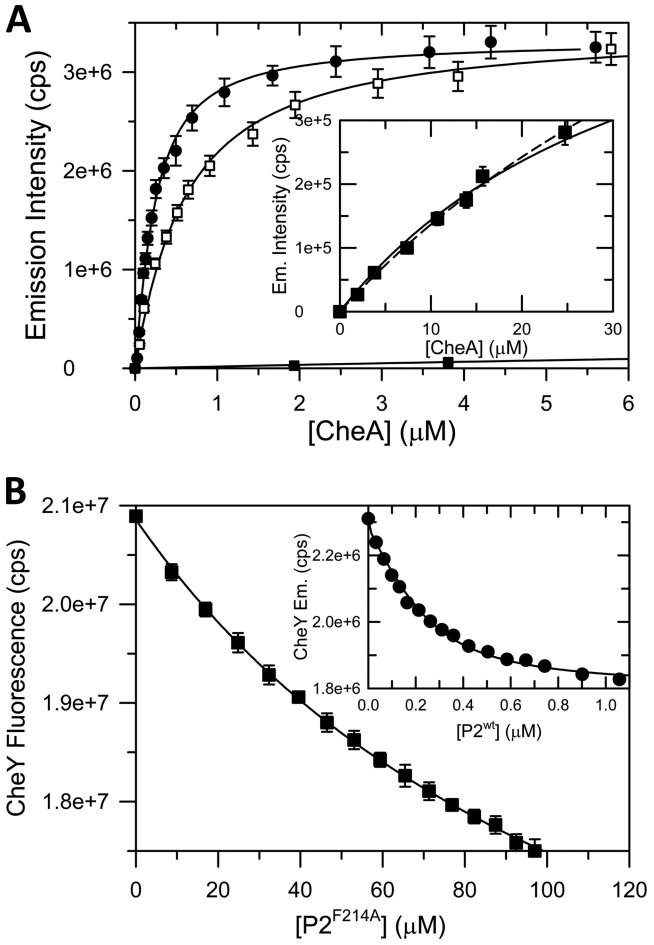

FIG. 2. Binding of wild-type and mutant CheA proteins to CheY. (A) Results of fluorescence-monitored titration of $CheY_{bd}$ (0.15 μM in 1-cm cuvettes) with $CheA_{wt}$ (●), CheA(E171A) (□), and CheA(F214A) (■); solid lines represent the best fit generated by least-squares analysis (DynaFit [25]) and indicate a K_d of 0.17 μM for $CheA_{wt}$, a K_d of 0.52 μM for CheA(E171A), and a K_d of 80 μM for CheA(F214A). The inset shows the CheA(F214A) titration extended to higher protein concentrations; the solid line shows the best fit obtained when both K_d and the molar fluorescence coefficient (F_{AY}) of the CheA-CheY complex were allowed to float in DynaFit (best fit K_d = 70 μM), and the dashed line shows the best fit obtained when only K_d was allowed to float while F_{AY} was fixed at the value observed with $CheA_{wt}$ (best fit K_d = 90 μM). (B) Results of fluorescence-monitored titration of 2.5 μM CheY (in 0.4-cm cuvettes) with P2(F214A) (main panel) and titration of 0.1 μM CheY (in 1-cm cuvettes) with $P2_{wt}$ (inset). The solid lines represent the best fit of the data obtained by least-squares analysis and indicated K_d values of 125 μM and 0.085 μM for P2(F214A) and $P2_{wt}$, respectively.

effects of our Ala substitutions on CheA-CheY binding energy and also summarizes the effects predicted by four different computer programs that were developed to identify hot spots at protein-protein binding interfaces.

Effect of F214A on CheA-CheY phosphotransfer kinetics. Because CheA(F214A) binds CheY so weakly, we anticipated that phosphotransfer from P-CheA(F214A) to CheY would be considerably slower than CheY phosphorylation by P-$CheA_{wt}$. To test this prediction, we used stopped-flow fluorescence experiments as described in previous work (32): the rapid decrease in fluorescence following mixing of P-CheA with CheY reflects decreased emission signal from CheY residue W58 as the protein becomes phosphorylated (on D57). Our results (Fig. 4) indicated that the CheA-CheY phosphotransfer kinetics are indeed markedly slower with CheA(F214A) than with $CheA_{wt}$ (15-fold slower at 8°C and 10-fold slower at 25°C [results not shown]). However, the observed 10-fold difference is somewhat less than one would predict, considering the 1,000-fold weaker binding affinity of CheA(F214A). Under these conditions, the minimal reaction describing the phosphotransfer reaction is P-CheA + CheY $\rightleftharpoons$ P-CheA-CheY $\rightharpoonup$ CheA + P-CheY, with rate constants k_1 (~10 μM^{-1} s^{-1}) and k_{-1} (~20 s^{-1}) for the forward and reverse steps of the binding reaction, and k_2 (250 s^{-1}) is the rate constant for phosphotransfer within the P-CheA-CheY complex (rate constants given here are for $CheA_{wt}$ at 8°C and are based on previous work [55, 56]). With $CheA_{wt}$, these rate constants predict a K_m of 27 μM for the phosphotransfer reaction. For a reaction involving 5 μM CheY, one would predict phosphotransfer to take place with a $k_{observed}$ value of 46 s^{-1}, which matches the $CheA_{wt}$ results shown in Fig. 4. For CheA(F214A), the diminished binding affinity could indicate a 1,000-fold decrease in k_1 or a 1,000-fold increase in k_{-1}, either of which would cause a significant increase in K_m, resulting in a value of 25,000 μM or 2,000 μM, respectively. For the experiment represented in Fig. 4, these values lead to a predicted $k_{observed}$ of 0.05 s^{-1} or 0.625 s^{-1}, respectively, which are significantly lower than the experimentally observed value (3 s^{-1}). This difference may provide some insight into the mechanisms of the CheA(F214A) → CheY phosphotransfer reaction (considered in Discussion).

Effects of F214A on polar localization of CheY-YFP in *E. coli*. The chemotaxis signaling proteins of *E. coli* form large clusters in which tens of thousands of receptor proteins gather in assemblies that also include most of the cell's CheA, CheY, CheZ, CheW, CheR, and CheB (31, 48, 50). These large (~200-nm), multiprotein assemblies are usually located at one or both poles of the cell (49, 71). Each cluster functions as a complex, highly cooperative signal processing unit, generating P-CheY that then dissociates from the cluster and diffuses to the flagellar motors, which are distributed at various locations

TABLE 1. Affinities of CheA Ala substitution mutants for CheY

Protein	K_d (μM)[a]
Full-length CheA	
wt	0.17 ± 0.02
E171A	0.57 ± 0.05
E178A	0.50 ± 0.05
H181A	0.18 ± 0.04
D202A	0.15 ± 0.05
D207A	0.20 ± 0.04
C213A	0.24 ± 0.04
F214A	80 ± 40
I216A	0.35 ± 0.05
P2 domain	
wt	0.09 ± 0.02
F214A	120 ± 20

[a] Results are means ± standard deviations for 2 or 3 independent experiments for mutants and 6 experiments for $CheA_{wt}$. Experiments with full-length CheA represent titrations of $CheY_{bd}$, while those with the isolated P2 domain represent titrations of unlabeled CheY.

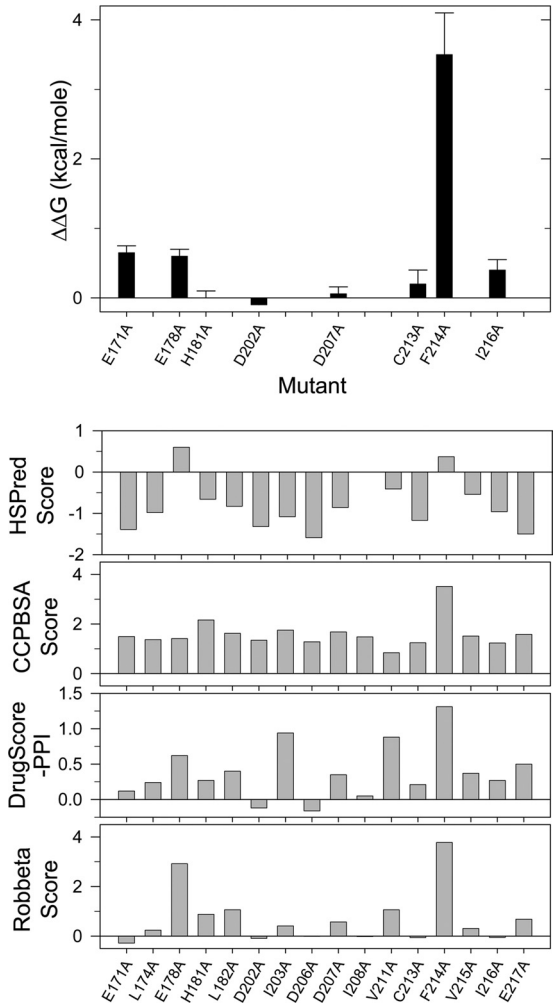

FIG. 3. Observed and predicted effects of alanine substitutions on the binding energy of the CheA-CheY complex. The top panel shows the experimental results, with ΔΔG values calculated using the ratio $K_{d\ \mathrm{mutant}}/K_{d\ \mathrm{wt}}$. The lower panels show predictions made by the following: the Robetta Ala-scanning server at the Baker laboratory (http://robetta.bakerlab.org/) (in kcal/mole) (38), the DrugScore^{PPI} Web server at the University of Dusseldorf (http://cpclab.uni-duesseldorf.de/dsppi/) (in kcal/mole) (24), the CCPBSA server (http://ccpbsa.biologie.uni-erlangen.de/) (in kcal/mole) (3), and the University College of London HSPred server (http://bioinf.cs.ucl.ac.uk/hspred) (in dimensionless units; a score of >0 indicates a hot spot, and a score of <0 indicates that the position is not a hot spot) (29). Predictions used subunits A and C of the PDB file 1EAY as input.

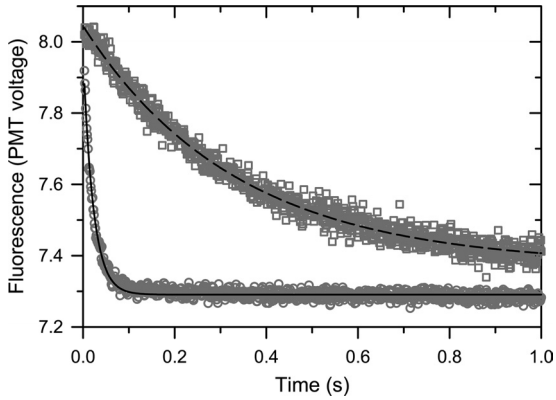

FIG. 4. Kinetics of phosphotransfer from P-CheA$_{wt}$ and P-CheA(F214A) to CheY. Stopped-flow experiments were performed to monitor the time course of fluorescence change after CheY (5 μM after mixing) was mixed with either P-CheA$_{wt}$ (○) or P-CheA(F214A) (□) (1 μM after mixing). Temperature (8°C) and buffer conditions (TNKGDG) match those used for binding titrations (Fig. 2 and Table 1). The lines represent the best fits of the data to a single-exponential decay, indicating a k_{observed} value of 45 s^{-1} for P-CheA$_{wt}$ (solid line) and a k_{observed} value of 3 s^{-1} for P-CheA(F214A) (dashed line). PMT, photomultiplier tube.

around the circumference of the cell (11, 48). These signal clusters are readily observed by fluorescence microscopy when GFP-tagged versions of the Che proteins are expressed in cells (50). We used CheY-EYFP and CheZ-ECFP to examine whether our CheA alanine substitutions affected formation of signal clusters or recruitment of CheY/CheZ into the clusters. Our results (Fig. 5 and additional results not shown) indicated that CheA(F214A) is defective in recruiting CheY-EYFP into the signal clusters, but the other CheA variants are not. We also observed that localization of CheZ-ECFP is not affected by F214A or any of the other mutations in P2. These results suggest that, in these experiments, the primary docking site for CheY in signal clusters is the P2 module of CheA. Previous work (60) had indicated that both CheZ and CheA can recruit CheY to the signal clusters but that CheZ-CheY interaction is primarily responsible for CheY recruitment in wild-type cells, while CheA-CheY interaction is responsible for CheY recruitment in the absence of CheZ. In view of those observations, it seems unlikely that F214A could cause defects in CheY-EYFP localization in a CheZ-replete cell. Therefore, it seems likely that our expression plasmid for CheY-EYFP and CheZ-ECFP generated CheZ-ECFP levels that were lower than the CheZ level in wild-type cells and that this created a situation that made it possible to visualize the effect of the F214A mutation.

Effects of Ala substitutions on chemotaxis ability of cells. We investigated the ability of all eight mutant versions of CheA (expressed using plasmid pAH1cheA) to support chemotaxis when expressed in Δ*cheA* cells growing in motility agar. We included in this analysis an additional mutant protein (CheAΔP2) that lacked the entire P2 domain (19). These results (Table 2) indicate that CheA(F214A) is less effective than CheA$_{wt}$, but the severity of this phenotype is not as extreme as that observed for CheAΔP2. The remaining Ala substitution mutants support chemotaxis ability comparable to that observed with CheA$_{wt}$.

We also used motility agar assays to investigate the effect of the F214A substitution when cells expressed *cheY* and *cheZ* at suboptimal levels. The underlying rationale here was that we could decrease CheY levels to a point where CheA → CheY phosphotransfer became rate limiting for the overall signaling pathway and that this would allow us to visualize more effectively the effects of a mutation affecting CheA-CheY interactions. For these experiments, two compatible plasmids were introduced into Δ*cheA* Δ*cheYZ E. coli* host cells: plasmid pAH1cheA expressed wt *cheA* or *cheA*(*F214A*) under the control of the *lac* promoter/operator, and plasmid pHK5 expressed *cheY-eyfp* and *cheZ-ecfp* under the control of a salicylate-inducible promoter (using CheY-YFP and CheZ-CFP in

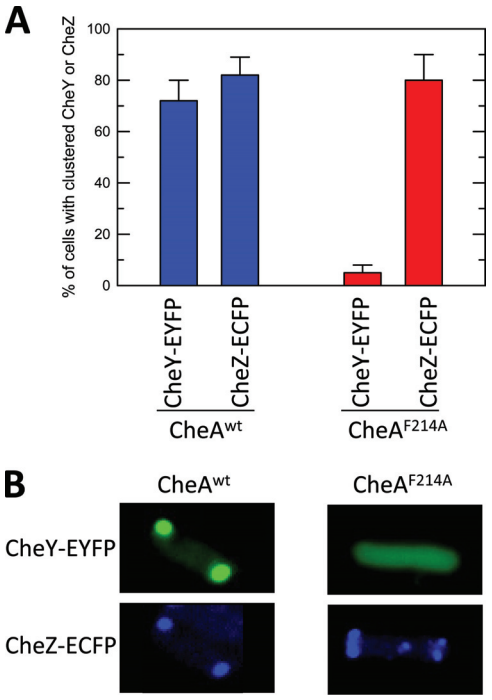

FIG. 5. Clustering of CheY-EYFP and CheZ-ECFP in *E. coli* cells expressing CheA(F214A) or $CheA_{wt}$. Fluorescent fusion proteins were expressed in strain NH1 (Δ*cheA* Δ*cheYZ*) using plasmid pHK5; CheA was expressed using the compatible plasmid pAH1cheA. The inducer concentrations were 1 μM salicylate and 5 μM IPTG. (A) At least 100 cells of each type were viewed using a fluorescence microscope and classified as either having or lacking a cluster(s) of fluorescent protein. Results reflect averages for experiments with two separate sets of transformants performed on different days, and the error bars represent the standard deviations. (B) Fluorescence images of a typical $CheA_{wt}$ cell and a typical CheA(F214A) cell (i.e., exhibiting the most common clustering/nonclustering phenotype).

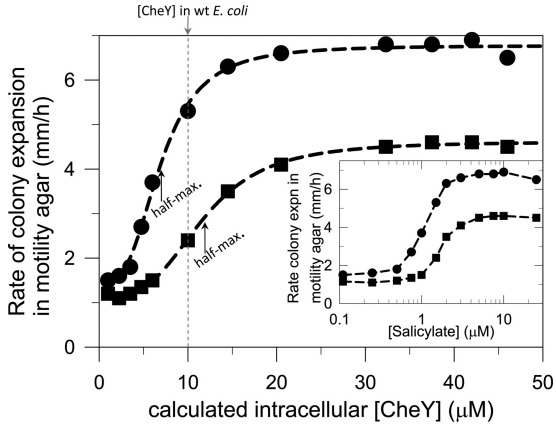

FIG. 6. Effect of F214A on chemotaxis ability in motility agar plates. NH1 cells (Δ*cheA* Δ*cheYZ*) carried plasmid pHK5 and plasmid pAH1cheA (wt or F214A). Motility agar plates were inoculated with 2-μl aliquots of saturated overnight broth cultures, and the rate of expansion of the diameter of each "swarm colony" was then measured over the ensuing 8 to 10 h. Plates contained 5 μM IPTG and salicylate concentrations ranging from 0 to 25 μM, as well as ampicillin and chloramphenicol to ensure maintenance of the plasmids. In a parallel experiment (using the same overnight cultures as the inoculum), broth cultures (at various salicylate concentrations) were grown to mid-log phase and used to record fluorescence emission spectra to quantify CheY-EYFP levels. This information was used to define the average intracellular concentration of CheY-EYFP at each salicylate concentration. ●, results for cells expressing $CheA_{wt}$; ■, results for cells expressing CheA(F214A). The lines represent the best (least-squares) fit of the data to a version of the Hill equation in SigmaPlot. This analysis indicated half-maximal activity at 6.9 ± 0.2 μM CheY (marked by ↑) and a Hill coefficient (N_H) of 3.0 ± 0.3 for $CheA_{wt}$ cells, while for cells expressing CheA(F214A), the values were 11.8 ± 0.2 μM CheY (marked by ↑) and an N_H of 3.3 ± 0.2. The inset shows the same results, but plotted using inducer (salicylate) concentration as the *x* axis; lines here are provided to facilitate viewing and do not reflect any modeling or curve-fitting analysis.

lieu of CheY and CheZ facilitated quantitation of expression levels and allowed us to correlate swarm assay results with FRET assay results [see below]). For these experiments, *cheA* expression was held constant (using 5 μM IPTG), and expression of *cheY-eyfp* and *cheZ-ecfp* was varied using a range of salicylate concentrations that resulted in CheY-EYFP protein levels ranging from 10 to 500% of the levels of CheY found in wild type *E. coli* (quantitation explained in Materials and Methods). The results of these experiments (Fig. 6) indicated that CheA(F214A) has a more severe defect when the levels of CheY (and CheZ) are lower than their wild-type levels. To illustrate this point, it is useful to compare the CheA-dependent swarm rate (the observed expansion rate for the swarm edge minus the "background" colony expansion rate in the absence of any CheA [1.1 mm/h]). At 10 μM CheY (the approximate CheY concentration in wild-type *E. coli*), the CheA-dependent swarm rate with $CheA_{wt}$ is approximately 3-times that observed with CheA(F214A). At 5 μM CheY, this comparison indicates a 6-fold difference between $CheA_{wt}$ and CheA(F214A).

Graphical analysis of the relationship between chemotaxis (swarm plate) ability and *cheYZ* expression level revealed a sigmoidal dependence (Fig. 6) in which the CheY level required for half-maximal activity was almost 2-fold higher for the CheA(F214A) mutant than for $CheA_{wt}$. This result supports the overall conclusion that the decreased chemotaxis ability observed for CheA(F214A) cells in swarm plates involves diminished CheY-CheA interactions and that this de-

TABLE 2. Abilities of mutant CheA proteins to support chemotaxis in motility agar

CheA variant[a]	Colony expansion rate on motility agar[b]
Wild type	1.0
No CheA	0.060 ± 0.007
ΔP2	0.16 ± 0.03
E171A	0.90 ± 0.07
E178A	0.9 ± 0.1
H181A	1.0 ± 0.1
D202A	0.84 ± 0.07
D207A	0.9 ± 0.1
C213A	1.0 ± 0.1
F214A	0.60 ± 0.07
I216A	0.90 ± 0.06

[a] Assays were performed using *E. coli* strain RP9538 (Δ*cheA*) transformed with plasmid pAH1 carrying the indicated *cheA* alleles. The "no CheA" plasmid had *eyfp* inserted in place of *cheA* in pAH1. The ΔP2 mutation was created by Jahreis et al. (19) and has an 11-amino-acid proline/alanine-rich linker in place of the P2 domain (amino acids 150 to 247 replaced).

[b] Results are means ± standard deviations for 3 or 4 independent experiments, normalized relative to the migration rate of RP9538/pAH1cheA[wt] on the same motility agar plate.

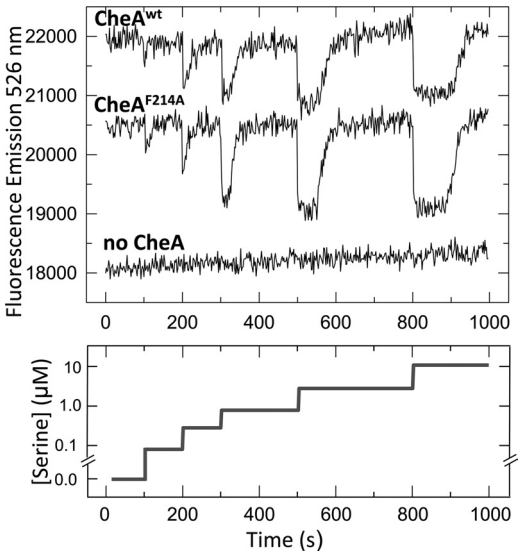

FIG. 7. FRET-monitored intracellular regulation of P-CheY levels in response to chemoattractant. Host cells (Δ*cheA* Δ*cheYZ*) carried plasmid pHK5 and plasmid pAH1cheA (wt or F214A). Cells collected from log-phase broth cultures (grown in the presence of 2 μM salicylate and 5 μM IPTG) were placed in a fluorescence cuvette in motility buffer and stimulated by stepwise addition of L-serine (the cumulative concentration is plotted in the bottom panel: the addition times were 100 s, 200 s, 300 s, 500 s, and 800 s). ECFP was excited ($\lambda_{excitation}$, 425 nm), and the EYFP emission signal ($\lambda_{emission}$, 526 nm) was monitored and interpreted as described in Materials and Methods.

fect causes a more extreme phenotype when intracellular CheY levels are lower than normal. It is unlikely that the decreased chemotaxis ability of CheA(F214A) results from any effect on CheA autokinase activity, as we observed normal autophosphorylation kinetics with purified CheA(F214A) (results not shown), and previous work demonstrated that completely eliminating the P2 domain does not have an adverse effect on CheA autophosphorylation (22).

Effects of Ala substitutions on *in vivo* signaling monitored using FRET assays. We adapted the FRET assay developed by Sourjik and Berg (51, 52) to monitor regulation of CheY phosphorylation levels in living *E. coli* cells. This assay utilizes CheY fused to EYFP and CheZ fused to ECFP. When phosphorylated, CheY-EYFP binds tightly to CheZ-ECFP, and this interaction generates a FRET signal. When CheY-YFP is dephosphorylated, the CheY-EYFP–CheZ-ECFP complex dissociates (because the affinity of CheZ for CheY is diminished), and the FRET signal disappears. This signal can be used to monitor changes in CheY phosphorylation levels taking place in cells when they are exposed to chemoattractants and repellents. Although this assay was initially developed using cells attached to microscope slides, we adapted it to monitor the FRET signal generated by cell suspensions maintained in standard fluorescence cuvettes and monitored using a standard steady-state spectrofluorometer (Fig. 7). In the absence of CheA, there is no observable modulation of CheY phosphorylation (FRET signal) when cells are exposed to chemotaxis stimuli, as expected. When expressed at wild-type levels using a regulated expression plasmid, $CheA_{wt}$ restored signaling ability to a Δ*cheA* strain. Using this assay, we examined the abilities of $CheA_{wt}$ and our Ala substitution versions of CheA to mediate regulation of CheY phosphorylation in response to successive additions of chemoattractant ranging from 0.1 to 10 μM; our results were similar to those reported by Sourjik and coworkers (51, 52): the FRET signal fell rapidly after cells were exposed to a chemoattractant and then gradually returned to the prestimulus level as a result of sensory adaptation (mediated by adjustments of receptor methylation levels by CheR and CheB). The extent of decrease of the FRET signal (P-CheY level) following attractant addition and the time required for adaptation were sensitive to the concentration of the attractant (Fig. 7). In these assays, each of the CheA variants supported normal excitation and adaptation time courses and exhibited sensitivities comparable to that observed with cells expressing $CheA_{wt}$. Surprisingly, this normal signaling ability was even observed with CheA(F214A) (Fig. 7). This robust signaling and adaptation were observed for CheA(F214A) cells responding to a variety of attractant stimuli (L-aspartate, α-methylaspartate, glucose, and γ-aminobutyric acid; results not shown) in addition to the serine experiment represented in Fig. 7, and it was observed over a range of CheY and CheZ expression levels (salicylate [inducer] concentrations ranging from 2 to 10 μM). We attempted to monitor the FRET signal for cells grown at lower inducer concentrations (e.g., 1 or 1.5 μM) for which the largest differences in swarm plate abilities were observed (Fig. 6); however, under these low-expression conditions, we could not observe any regulation of the small EYFP signal in either $CheA_{wt}$ cells or CheA(F214A) cells.

DISCUSSION

F214 in the P2 domain of CheA is a hot-spot and anchor residue. Protein-protein binding interfaces can be represented as discrete clusters of closely interacting residues (40). High-affinity complexes (K_ds in the nM or pM range) appear to utilize multiple clusters that are "highly developed" (have numerous interconnected contact points). In contrast, the P2-CheY complex utilizes only one medium-sized developed cluster and therefore has comparatively weak affinity. As depicted in Fig. 1C (and Fig. 4 in reference 40), F214 is a central hub in this cluster, and so it is not surprising that the F214A mutation has a major effect on binding affinity: there are no additional cluster modules to promote binding when the F214 cluster loses its central hub.

Amino acid side residues that participate in key contacts between the binding partners are often referred to as "hot spot" residues (6, 10, 18), and they can be identified by scanning mutagenesis experiments such as those reported here: a substitution of alanine for a hot spot residue has a large negative impact on the affinity of the binding interaction, and the magnitude of this effect can be expressed as ΔΔG (14, 43). Often, a ΔΔG value of 2 kcal/mole is used as the cutoff for hot-spot designation (34, 59), although sometimes a distinction is made between "warm-spot" positions (1 kcal/mole $<$ ΔΔG $<$ 4 kcal/mole) and hot-spot positions (ΔΔG $>$ 4 kcal/mole) (35, 36). The severely weakened binding affinity of CheA(F214A) indicates that F214 is an important contributor to the CheA-CheY binding interaction and identifies F214 as a hot-spot residue (or a very warm spot). This observation confirms predictions (Fig. 3) made by several computer programs designed

to analyze protein-protein interfaces and identify hot spots: these programs predict that F214 contributes 1.3 to 3.8 kcal/mol to the binding energy, roughly matching our experimental observations ($\Delta\Delta G$, ~3.7 to 4.1 kcal mole^{-1}). The *in silico* alanine-scanning predictions made by some of these programs also identified several other P2 positions as potential hot spots (E178, H181, and D207); however, our results do not support these predictions.

A different method for *in silico* analysis of protein-protein binding interfaces was devised by Rajamani et al. (37). When applied to a CheY-P2 crystal structure, this method identified F214 as the key "anchor residue" in the binding interface. Such an anchor residue can be found in many protein-protein interfaces; each anchor serves as a key organizing center around which other "latch" interactions are assembled via induced-fit conformational changes, presumably after the anchor has been situated properly. From this perspective, one can think of P2 residue F214 being maintained in a ready-to-bind conformation that fits into an accommodating recognition surface on CheY, and this promotes several latch interactions (involving CheY lysine side chains interacting with P2 glutamate side chains). Among the predicted P2 latch sites are the side chains of E171 and E217 in P2 (37). Our results indicate that one of the latches (E171) makes a small contribution to the binding energy, as does E178, a possible alternative latch residue (we did not examine E217 in this study).

The relatively small contributions of the P2-CheY latch sites to the overall binding energy suggest that "unlatching" would be relatively easy, such that a complex anchored via F214 could sample several alternative conformations (utilizing different latches). The possibility of conformational plasticity has been raised previously to account for the observation of several alternative interface structures in CheY-P2 crystals (33) and for the rapid kinetics of complex assembly (55).

Consequences of F214A for the CheA → CheY phosphotransfer mechanism. Our results demonstrate that the CheA → CheY phosphotransfer reaction is markedly slower with CheA(F214A) than with $CheA_{wt}$. However, at first glance, the magnitude of this effect (~10-fold) is not as large as the 70- to 900-fold effect one would predict for a CheA protein with 1,000-fold-lower affinity for CheY. This discrepancy might result from CheY bypassing P2 binding and interacting directly with the phosphorylated P1 domain of P-CheA(F214A). Indeed, in previous work we observed that CheY can acquire a phosphoryl group from a mutant version of CheA that completely lacks the P2 domain, albeit with reduced catalytic efficiency (54). Therefore, it seems likely that CheY adopts such a mechanism with CheA(F214A) and that this allows CheA(F214A) → CheY phosphotransfer to take place at a rate of ~10% of that observed with $CheA_{wt}$, which would indicate an effective second-order rate constant of ~10 μM^{-1} s^{-1}. This value indicates that P-CheA(F214A) is somewhat more effective than P-CheAΔP2 (k_{phos}, ~1.5 μM^{-1} s^{-1}) (54) and considerably more effective than small-molecule phosphodonors such as phorphoramidate and acetyl phosphate, for which k_{phos} is 10^{-5} to 10^{-4} μM^{-1} s^{-1} (32). The latter comparison supports the idea that P1 must make important contributions to the kinetics of phosphotransfer, although the nature of these contributions have yet to be defined (54).

Consequences of F214A for chemotaxis signal transduction in cells. Here, we consider (i) the predicted effects of decreased phosphotransfer kinetics of CheA(F214A) on the overall ability of the chemotaxis system to regulate CheY phosphorylation and (ii) why these predictions do not match our experimental observations. One simple way of making semiquantitative predictions of the effect of F214A is to consider the rate of the phosphotransfer step relative to other key steps that affect P-CheY levels. In wild-type cells, the CheA → CheY phosphotransfer step (200 to 500 s^{-1}) is considerably faster than the CheA autophosphorylation reaction (~20 to 50 s^{-1}) and faster than the CheY dephosphorylation reaction (~50 to 100 s^{-1} for the CheZ-catalyzed reaction), but the situation is somewhat different for CheA(F214A): with this mutant protein, autophosphorylation, phosphotransfer, and dephosphorylation would take place at roughly equivalent rates. The relative magnitudes of these steps dictate the steady-state level of P-CheY, and their absolute magnitudes define how rapidly P-CheY levels can be adjusted when changes in CheA autokinase activity are orchestrated by the chemotaxis receptor proteins. For $CheA_{wt}$, simple modeling (see Materials and Methods) using current best estimates of rate constants and protein concentrations predicts that, in an average *E. coli* cell, there is a steady-state P-CheY concentration of ~3.1 μM (~30% of the total CheY pool) and that this can be quickly adjusted downward in response to an attractant stimulus (half-life [$t_{1/2}$], ~0.03 s). For CheA(F214A), our results predict that the steady-state level of CheY-P would be ~1.9 μM and the $t_{1/2}$ ~0.045 s for an attractant response. Thus, we expected that our FRET experiments would show a decreased range of responsiveness (less P-CheY to deplete) for the CheA(F214A) cells exposed to a saturating attractant stimulus. Our FRET assay results (Fig. 7) did not match this prediction.

We considered the possibility that our "basic model" (above) was too simple to accurately represent signaling in a cell. A much more sophisticated approach for predicting the effects of the CheA(F214A) mutation is to utilize the RapidCell model developed by Vladimirov et al. (61, 62). This model takes into account essentially all of the known features of the *E. coli* chemotaxis system and can use this information to simulate expected time courses of intracellular P-CheY levels when cells are subjected to stepwise increases and decreases of attractant stimuli. Using the default (wild-type) settings for rate constants and protein concentrations, we generated the simulated time course shown in Fig. 8 for cells exposed to addition of a chemoattractant and then to removal of this attractant. Repeating this simulation using progressively lower values of k_{phos} predicts progressively lower steady-state levels (prestimulus) of P-CheY and corresponding decreases in the magnitudes of responses (change in P-CheY levels after attractant addition or removal). Based on these simulations, we expected that we would have been able to detect a 4-fold change in k_{phos} and that a 10-fold decrease in this rate constant would result in a very noticeable decrease in response magnitude. However, our experimental observations did not match these predictions.

This disagreement raises the possibility that some aspect of the *in vivo* signaling system compensates for the slow phosphotransfer kinetics of CheA(F214A). For example, there could be changes in the methylation status of the chemotaxis receptor

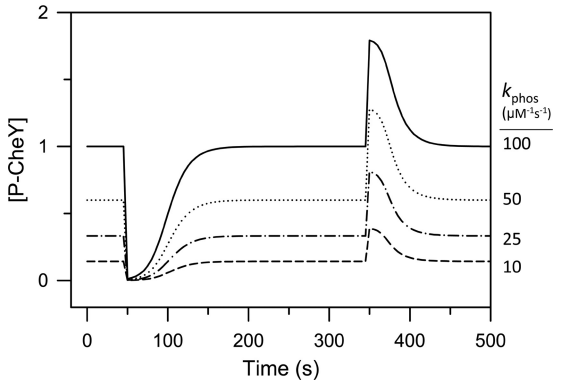

FIG. 8. Computer simulations of chemotaxis responses. RapidCell version 1.2.3 (61, 62) simulated the P-CheY levels in cells exposed to an instantaneous stepwise addition of attractant (from 0 to 30 μM) at 50 s and then to stepwise removal of this attractant at 350 s. The K_d of the chemoreceptor for the attractant was set at 40 μM. The top (solid) line shows the simulation results obtained using the default values for rate constants and protein concentrations. The bottom (dashed) line shows the results obtained when the effective second-order rate constant for CheA → CheY phosphotransfer was decreased 10-fold. The first segments of these time courses (0 to 200 s) correspond to the stepwise responses we monitored in Fig. 7.

proteins that alter their signaling activities in a manner that overcomes this defect (19). Alternatively, in the context of the full chemotaxis system, the F214A mutation might give rise to a compensatory decrease of the steady-state phosphatase activity of CheZ such that the intracellular P-CheY concentration is poised at an effective level.

ACKNOWLEDGMENTS

We thank Sandy Parkinson for strains and plasmids, Victor Sourjik for providing the *eyfp* and *ecfp* plasmids, which served as starting points for generating our fusions, Steve Wolniak for help with fluorescence microscopy, and Ricaele VanBruggen and Ebele Okwumabua for protein purification assistance.

S.N. gratefully acknowledges support from a Howard Hughes Undergraduate Research Fellowship at the University of Maryland.

This work was supported by Public Health Service grant GM052853 to R.C.S. from the National Institute of General Medical Sciences.

REFERENCES

1. **Ames, P., C. A. Studdert, R. H. Reiser, and J. S. Parkinson.** 2002. Collaborative signaling by mixed chemoreceptor teams in *Escherichia coli*. Proc. Natl. Acad. Sci. U. S. A. **99:**7060–7065.
2. **Baker, M. D., P. M. Wolanin, and J. B. Stock.** 2006. Signal transduction in bacterial chemotaxis. Bioessays **28:**9–22.
3. **Benedix, A., C. M. Becker, B. L. de Groot, A. Caflisch, and R. A. Bockmann.** 2009. Predicting free energy changes using structural ensembles. Nat. Methods **6:**3–4.
4. **Bilwes, A. M. P., C. M. Quezada, M. Simon, and B. R. Crane.** 2003. Structure and function of CheA, the histidine kinase central to bacterial chemotaxis, p. 48–74. *In* M. Inouye and R. Dutt. (ed.), Histidine kinases in signal transduction. Academic Press, San Diego, CA.
5. **Block, S. M., J. E. Segall, and H. C. Berg.** 1982. Impulse responses in bacterial chemotaxis. Cell **31:**215–226.
6. **Bogan, A. A., and K. S. Thorn.** 1998. Anatomy of hot spots in protein interfaces. J. Mol. Biol. **280:**1–9.
7. **Borkovich, K. A., and M. I. Simon.** 1990. The dynamics of protein phosphorylation in bacterial chemotaxis. Cell **63:**1339–1348.
8. **Brissette, P., D. P. Ballou, and V. Massey.** 1989. Determination of the dead time of a stopped-flow fluorometer. Anal. Biochem. **181:**234–238.
9. **Buron-Barral, M., K. K. Gosink, and J. S. Parkinson.** 2006. Loss- and gain-of-function mutations in the F1-HAMP region of the *Escherichia coli* aerotaxis transducer Aer. J. Bacteriol. **188:**3477–3486.
10. **Clackson, T., and J. A. Wells.** 1995. A hot-spot of binding-energy in a hormone-receptor interface. Science **267:**383–386.
11. **Cluzel, P., M. Surette, and S. Leibler.** 2000. An ultrasensitive bacterial motor reveled by monitoring signaling proteins in single cells. Science **287:**1652–1655.
12. **Datsenko, K. A., and B. L. Wanner.** 2000. One-step inactivation of chromosomal genes in *Escherichia coli* K-12 using PCR products. Proc. Natl. Acad. Sci. U. S. A. **97:**6640–6645.
13. **Eaton, A. K., and R. C. Stewart.** 2009. The two active sites of *Thermotoga maritima* CheA dimers bind ATP with dramatically different affinities. Biochemistry **48:**6412–6422.
14. **Fersht, A.** 1999. Structure and mechanism in protein science. W. H. Freeman and Co., New York, NY.
15. **Hess, J. F., R. B. Bourret, K. Oosawa, P. Matsumura, and M. I. Simon.** 1988. Protein phosphorylation and bacterial chemotaxis. Cold Spring Harbor Symp. Quant. Biol. **53:**41–48.
16. **Hess, J. F., K. Oosawa, N. Kaplan, and M. I. Simon.** 1988. Phosphorylation of three proteins in the signaling pathway of bacterial chemotaxis. Cell **53:**79–87.
17. **Hirschman, A., M. Boukhvalova, R. VanBruggen, A. J. Wolfe, and R. C. Stewart.** 2001. Active site mutations in CheA, the signal-transducing protein kinase of the chemotaxis system in *Escherichia coli*. Biochemistry **40:**13876–13887.
18. **Hu, Z. J., B. Y. Ma, H. Wolfson, and R. Nussinov.** 2000. Conservation of polar residues as hot spots at protein interfaces. Proteins **39:**331–342.
19. **Jahreis, K., T. B. Morrison, A. Garzon, and J. S. Parkinson.** 2004. Chemotactic signaling by an *Escherichia coli* CheA mutant that lacks the binding domain for phosphoacceptor partners. J. Bacteriol. **186:**2664–2672.
20. **Johnson, K. A., Z. B. Simpson, and T. Blom.** 2009. Global kinetic explorer: a new computer program for dynamic simulation and fitting of kinetic data. Anal. Biochem. **387:**20–29.
21. **Kentner, D., and V. Sourjik.** 2009. Dynamic map of protein interactions in the *Escherichia coli* chemotaxis pathway. Mol. Syst. Biol. **5:**238.
22. **Khan, S., S. Jain, G. P. Reid, and D. R. Trentham.** 2004. The fast tumble signal in bacterial chemotaxis. Biophys. J. **86:**4049–4058.
23. **Kollmann, M., L. Lovdok, K. Bartholome, J. Timmer, and V. Sourjik.** 2005. Design principles of a bacterial signalling network. Nature **438:**504–507.
24. **Krüger, D. M., and H. Gohlke.** 2010. DrugScorePPI webserver: fast and accurate *in silico* alanine scanning for scoring protein-protein interactions. Nucleic Acids Res. **38:**W480–W486.
25. **Kuzmic, P.** 1996. Program DYNAFIT for the analysis of enzyme kinetic data: application to HIV proteinase. Anal. Biochem. **237:**260–273.
26. **Levit, M., Y. Liu, M. Surette, and J. Stock.** 1996. Active site interference and asymmetric activation in the chemotaxis protein histidine kinase CheA. J. Biol. Chem. **271:**32057–32063.
27. **Li, J., R. V. Swanson, M. I. Simon, and R. M. Weis.** 1995. The response regulators CheB and CheY exhibit competitive binding to the kinase CheA. Biochemistry **34:**14626–14636.
28. **Li, M., and G. L. Hazelbauer.** 2004. Cellular stoichiometry of the components of the chemotaxis signaling complex. J. Bacteriol. **186:**3687–3694.
29. **Lise, S., C. Archambeau, M. Pontil, and D. T. Jones.** 2009. Prediction of hot spot residues at protein-protein interfaces by combining machine learning and energy-based methods. BMC Bioinformatics **10:**365.
30. **Liu, J.** 1990. Molecular genetics of the chemotaxis signaling pathway in *Escherichia coli.* Ph.D. thesis. University of Utah, Salt Lake City, UT.
31. **Maddock, J. R., and L. Shapiro.** 1993. Polar location of the chemoreceptor complex in the *Escherichia coli* cell. Science **259:**1717–1723.
32. **Mayover, T. C., C. J. Halkides, and R. C. Stewart.** 1999. Kinetic characterization of CheY phosphorylation reactions: comparison of P-CheA and small-molecule phosphodonors. Biochemistry **38:**2259–2271.
33. **McEvoy, M. M., A. C. Hausrath, G. B. Randolph, S. J. Remington, and F. W. Dahlquist.** 1998. Two binding modes reveal flexibility in kinase/response regulator interactions in the bacterial chemotaxis pathway. Proc. Natl. Acad. Sci. U. S. A. **95:**7333–7338.
34. **Moreira, I. S., P. A. Fernandes, and M. J. Ramos.** 2007. Hot spots—a review of the protein-protein interface determinant amino-acid residues. Proteins **68:**803–812.
35. **Moreira, I. S., P. A. Fernandes, and M. J. Ramos.** 2006. Unraveling the importance of protein-protein interaction: application of a computational alanine-scanning mutagenesis to the study of the IgG1 streptococcal protein G (C2 fragment) complex. J. Phys. Chem. B **110:**10962–10969.
36. **Pons, J., A. Rajpal, and J. F. Kirsch.** 1999. Energetic analysis of an antigen/antibody interface: alanine scanning mutagenesis and double mutant cycles on the hyhel-10/lysozyme interaction. Protein Sci. **8:**958–968.
37. **Rajamani, D., S. Thiel, S. Vajda, and C. J. Camacho.** 2004. Anchor residues in protein-protein interactions. Proc. Natl. Acad. Sci. U. S. A. **101:**11287–11292.
38. **Raman, S., et al.** 2009. Structure prediction for CASP8 with all-atom refinement using Rosetta. Proteins **77:**89–99.
39. **Reichmann, D., et al.** 2007. Binding hot spots in the TEM1-BLIP interface in light of its modular architecture. J. Mol. Biol. **365:**663–679.
40. **Reichmann, D., et al.** 2005. The modular architecture of protein-protein binding interfaces. Proc. Natl. Acad. Sci. U. S. A. **102:**57–62.
41. **Sagi, Y., S. Khan, and M. Eisenbach.** 2003. Binding of the chemotaxis

response regulator CheY to the isolated, intact switch complex of the bacterial flagellar motor—lack of cooperativity. J. Biol. Chem. **278:**25867–25871.
42. **Sanders, D. A., B. L. Gillece-Castro, A. M. Stock, A. L. Burlingame, and D. E. Koshland, Jr.** 1989. Identification of the site of phosphorylation of the chemotaxis response regulator protein, CheY. J. Biol. Chem. **264:**21770–21778.
43. **Schreiber, G., and A. R. Fersht.** 1993. Interaction of banase with its polypeptide inhibitor barstar studied by protein engineering. Biochemistry **32:**5145–5150.
44. **Shaner, N. C., P. A. Steinbach, and R. Y. Tsien.** 2005. A guide to choosing fluorescent proteins. Nat. Methods **2:**905–909.
45. **Shukla, D., and P. Matsumura.** 1995. Mutations leading to altered CheA binding cluster on a face of CheY. J. Biol. Chem. **270:**24414–24419.
46. **Silversmith, R. E., M. D. Levin, E. Schilling, and R. B. Bourret.** 2008. Kinetic characterization of catalysis by the chemotaxis phosphatase CheZ. J. Biol. Chem. **283:**756–765.
47. **Smith, J. G., et al.** 2003. Investigation of the role of electrostatic charge in activation of the *Escherichia coli* response regulator CheY. J. Bacteriol. **185:**6385–6391.
48. **Sourjik, V.** 2004. Receptor clustering and signal processing in *E. coli* chemotaxis. Trends Microbiol. **12:**569–576.
49. **Sourjik, V., and J. P. Armitage.** 2010. Spatial organization in bacterial chemotaxis. EMBO J. **29:**2724–2733.
50. **Sourjik, V., and H. C. Berg.** 2000. Localization of components of the chemotaxis machinery of *Escherichia coli* using fluorescent protein fusions. Mol. Microbiol. **37:**740–751.
51. **Sourjik, V., and H. C. Berg.** 2002. Receptor sensitivity in bacterial chemotaxis. Proc. Natl. Acad. Sci. U. S. A. **99:**123–127.
52. **Sourjik, V., A. Vaknin, T. S. Shimizu, and H. C. Berg.** 2007. In vivo measurement by FRET of pathway activity in bacterial chemotaxis. Methods Enzymol. **423:**365–391.
53. **Stewart, R. C.** 1997. Kinetic characterization of phosphotransfer between CheA and CheY in the bacterial chemotaxis signal transduction pathway. Biochemistry **36:**2030–2040.
54. **Stewart, R. C., K. Jahreis, and J. S. Parkinson.** 2000. Rapid phosphotransfer to CheY from a CheA protein lacking the CheY-binding domain. Biochemistry **39:**13157–13165.
55. **Stewart, R. C., and R. Van Bruggen.** 2004. Association and dissociation kinetics for CheY interacting with the P2 domain of CheA. J. Mol. Biol. **336:**287–301.
56. **Stewart, R. C., and R. VanBruggen.** 2004. Phosphorylation and binding interactions of CheY studies by use of Badan-labeled protein. Biochemistry **43:**8766–8777.
57. **Swanson, R. V., et al.** 1995. Localized perturbations in CheY structure monitored by NMR identify a CheA binding interface. Nat. Struct. Biol. **2:**906–910.
58. **Szurmant, H., and G. W. Ordal.** 2004. Diversity in chemotaxis mechanisms among Bacteria and Archaea. Microbiol. Mol. Biol. Rev. **68:**301–319.
59. **Thorn, K. S., and A. A. Bogan.** 2001. ASEdb: a database of alanine mutations and their effects on the free energy of binding in protein interactions. Bioinformatics **17:**284–285.
60. **Vaknin, A., and H. C. Berg.** 2004. Single-cell FRET imaging of phosphatase activity in the *Escherichia coli* chemotaxis system. Proc. Natl. Acad. Sci. U. S. A. **101:**17072–17077.
61. **Vladimirov, N.** 2009. Multiscale modeling of bacterial chemotaxis. Ph.D. thesis. Ruperto-Carola University of Heidelberg, Heidelberg, Germany.
62. **Vladimirov, N., L. Lovdok, D. Lebiedz, and V. Sourjik.** 2008. Dependence of bacterial chemotaxis on gradient shape and adaptation rate. PLoS Comput. Biol. **4:**e1000242.
63. **Wadhams, G. H., and J. P. Armitage.** 2004. Making sense of it all: bacterial chemotaxis. Nat. Rev. Mol. Cell Biol. **5:**1024–1037.
64. **Welch, M., N. Chinardet, L. Mourey, C. Birck, and J.-P. Samama.** 1998. Structure of the CheY-binding domain of histidine kinase CheA in complex with CheY. Nat. Struct. Biol. **5:**25–29.
65. **Welch, M., K. Oosawa, S.-I. Aizawa, and M. Eisenbach.** 1994. Effects of phosphorylation, Mg^{+2}, and conformation of the chemotaxis protein CheY on its binding to the flagellar switch protein FliM. Biochemistry **33:**10470–10476.
66. **Welch, M., K. Oosawa, S.-I. Aizawa, and M. Eisenbach.** 1993. Phosphorylation-dependent binding of a signal molecule to the flagellar switch of bacteria. Proc. Natl. Acad. Sci. U. S. A. **90:**8787–8791.
67. **Wolfe, A. J., and H. C. Berg.** 1989. Migration of bacteria in semisolid agar. Proc. Natl. Acad. Sci. U. S. A. **86:**6973–6977.
68. **Wright, S., B. Walia, J. S. Parkinson, and S. Khan.** 2006. Differential activation of *Escherichia coli* chemoreceptors by blue-light stimuli. J. Bacteriol. **188:**3962–3971.
69. **Yen, K. M.** 1991. Construction of cloning cartridges for development of expression vectors in gram-negative bacteria. J. Bacteriol. **173:**5328–5335.
70. **Zacharias, D. A., J. D. Violin, A. C. Newton, and R. Y. Tsien.** 2002. Partitioning of lipid-modified monomeric GFPs into membrane microdomains of live cells. Science **296:**913–916.
71. **Zhang, P. J., C. M. Khursigara, L. M. Hartnell, and S. Subramaniam.** 2007. Direct visualization of *Escherichia coli* chemotaxis receptor arrays using cryo-electron microscopy. Proc. Natl. Acad. Sci. U. S. A. **104:**3777–3781.
72. **Zhou, H., and F. W. Dahlquist.** 1997. Phosphotransfer site of the chemotaxis-specific protein kinase CheA as revealed by NMR. Biochemistry **36:**699–710.
73. **Zhou, H. J., et al.** 1996. Phosphotransfer and CheY-binding domains of the histidine autokinase CheA are joined by a flexible linker. Biochemistry **35:**433–443.